Thermocapillary actuation of liquid flow on chemically patterned surfaces

Anton A. Darhuber, Jeffrey M. Davis, and Sandra M. Troian[a)]
*Microfluidic Research and Engineering Laboratory, Department of Chemical Engineering,
Princeton University, Princeton, New Jersey 08544*

Walter W. Reisner
Department of Physics, Princeton University, Princeton, New Jersey 08544

We have investigated the thermocapillary flow of a Newtonian liquid on hydrophilic microstripes which are lithographically defined on a hydrophobic surface. The speed of the microstreams is studied as a function of the stripe width w, the applied thermal gradient $|dT/dx|$ and the liquid volume V deposited on a connecting reservoir pad. Numerical solutions of the flow speed as a function of downstream position show excellent agreement with experiment. The only adjustable parameter is the inlet film height, which is controlled by the ratio of the reservoir pressure to the shear stress applied to the liquid stream. In the limiting cases where this ratio is either much smaller or much larger than unity, the rivulet speed shows a power law dependency on w, $|dT/dx|$ and V. In this study we demonstrate that thermocapillary driven flow on chemically patterned surfaces can provide an elegant and tunable method for the transport of ultrasmall liquid volumes in emerging microfluidic technologies. © *2003 American Institute of Physics.* [DOI: 10.1063/1.1562628]

I. INTRODUCTION

Various microfluidic systems are being developed to transport ultrasmall volumes of liquids through miniaturized network assemblies. Applications for these devices include species separation, DNA sequencing and combinatorial chemistry.[1–4] The integration of fluidic networks with devices for performing chemical reactions, separations and sequencing into a single ''lab-on-a-chip'' provides a highly parallel platform for automated handling and analysis of small fluid volumes, thereby minimizing waste volume and reagent cost.

Different transport mechanisms have been utilized in microfluidic devices including pressure gradients,[5] electrophoresis and electro-osmosis,[6] electrohydrodynamics,[7] magnetohydrodynamics,[8,9] centrifugation[10] and thermocapillary pumping (TCP).[11] The TCP technique uses heating elements exterior to a closed channel to modify the surface tension at one end of a liquid plug. The difference in temperature between the front and back ends generates a capillary pressure gradient for liquid propulsion. Electrophoresis and electroosmosis can also induce chemical separation in ionic solutions during transport. The majority of these techniques move either continuous streams or discrete droplets within enclosed networks.

There are only a few studies which target microfluidic delivery on open surfaces. Electrowetting[12,13] and dielectrophoresis[14] have been used to move or dispense discrete droplets on glass substrates using voltages between 10 and 1000 V. In this paper, we consider the use of thermocapillary forces and chemically patterned substrates for moving continuous streams and droplets on an open surface. The chemical patterning, which consists of surface regions that either attract or repel the liquid, laterally confines the liquid flow to selected pathways. Temperature gradients ∇T applied parallel to the solid surface induce thermocapillary stresses in the overlying liquid with subsequent flow from warm to cool regions of the solid. The chemical surface treatment defines all possible carrier pathways. The actual flow pathway is selected by activating electronically addressable thin film heaters. Programmable surface temperature maps therefore provide remote control over the direction, timing and flow rate on hydrophilic segments. The capability of manipulating liquid flow by tuning the local temperature provides a powerful and versatile approach to microfluidic delivery.

Advantages of this method of fluidic transport include no moving parts, low applied voltages and a wider spectrum of acceptable liquids. By contrast, electrokinetic techniques require strongly ionic liquids and high operating voltages. In addition, since the open architecture of the thermally driven device allows continuous contact of the liquid phase with the ambient gas phase, devices based on this concept can also be used as sensors and detectors for soluble gases, aerosols or airborne microscopic particles. Due to the high surface to volume ratio in such fluidic systems, the device is best suited to liquids of low volatility, although encapsulation can minimize evaporative losses during transport of moderately volatile samples.

In this article we present an experimental and theoretical study of the thermocapillary flow of continuous streams on hydrophilic microstripes subject to a constant thermal gradient. Linear temperature profiles are established by simultaneously heating and cooling opposite ends of a silicon substrate. Using this assembly, we study the dependence of the

[a)]Author to whom correspondence should be addressed. Electronic mail:
stroian@princeton.edu

flow speed on the stripe width w, the applied thermal gradient $|dT/dx|$ and the liquid volume V deposited on a reservoir pad. The lateral confinement of the flowing liquid to the microstripe causes a significant curvature of the liquid–air interface which contributes to the flow characteristics in ways not present in the thermocapillary flow of liquids on homogeneous surfaces. In fact, instabilities often observed in thermocapillary spreading[15–17] are suppressed by the additional transverse curvature. We develop scaling relations for two limiting cases in which the ratio of the reservoir pressure to the shear stress applied to the liquid stream is either much smaller or larger than unity. In these limits, the rivulet speed shows power law dependency on w, $|dT/dx|$ and V. Full numerical solutions of the flow speed as a function of downstream position, based on a lubrication model which includes thermocapillary stress, capillary forces and temperature dependent viscosity, show excellent agreement with experiment.

II. EXPERIMENTAL SETUP

Samples were prepared from n-type doped, $\langle 100 \rangle$-oriented silicon wafers with a nominal resistivity of 10–20 Ω cm and thermal conductivity $k_{Si} = 160$ W/mK at room temperature.[18] The samples were cleaned by immersion in acetone and isopropanol followed by a mixture of hydrogen peroxide (H_2O_2) and sulfuric acid (H_2SO_4) at $T = 80\,°C$.

For electrical passivation, the silicon samples were first coated with 200 nm silicon nitride (SiN_x) and 200 nm silicon oxide (SiO_2) using plasma enhanced chemical vapor deposition (PECVD) in a Plasmatherm 790 at $T = 250\,°C$. The SiN_x layer was deposited with N_2, NH_3 and SiH_4 at gas flow rates of 150, 2 and 110 sccm, respectively, at a chamber pressure of 900 mTorr and a power setting of 20 W. Operating parameters for the SiO_2 deposition layer were 160 sccm of N_2O and 35 sccm of SiH_4 at a chamber pressure of 400 mTorr and a power setting of 25 W. The metal heating resistors were deposited with a Denton electron beam evaporator and a photolithographic lift-off procedure. After metal evaporation, the resistors were covered with a 700 nm thick layer of PECVD SiO_2 deposited with the same parameter settings as above.

The sample surface was subsequently made hydrophobic by treatment with a self-assembled monolayer of 1H-, 1H-, 2H-, 2H-perfluorooctyl-trichlorosilane (PFOTS, Fluka)[19,20] and photolithography. This coating completely suppressed flow on the silanized regions for the liquids and the volumes used in this study. The monolayer thickness of about 3 nm is negligible on the scale of the film and flow geometry ($\gtrsim 10$ μm). The substrate surface can therefore be regarded as flat but chemically heterogeneous. The hydrophilic pattern, as shown in Fig. 1(a), consisted of pairs of square reservoirs, 4.5 mm per side, connecting 26 mm long hydrophilic stripes ranging in width from 100–800 μm. The volumetric flow rates in this study were rather small given the minute geometric dimensions. The reservoir volume therefore remained essentially constant for the duration of an experiment. A schematic diagram of the flow geometry is shown in
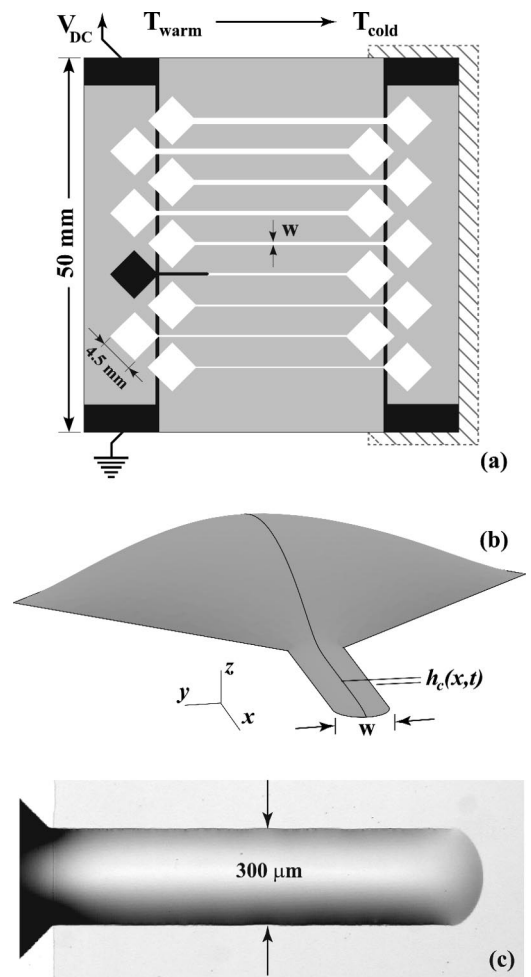

FIG. 1. (a) Diagram of the sample layout. White (grey) areas denote hydrophilic (hydrophobic) regions of the substrate. The liquid reservoirs are squares measuring 4.5 mm per side. The hatched rectangle on the right denotes the position of the cooling block. The black rectangles (3.6×10 mm^2) located at the sample corners represent the electrical contacts to the resistive metal heaters (black vertical stripes) which are located beneath the sample surface at the stripe inlets. (b) Schematic diagram of a liquid sample spreading from a reservoir onto a hydrophilic microstripe of width w. The x-coordinate axis coincides with the central axis of the microstripe; the z-axis lies perpendicular to the sample surface. The variable $h_c(x,t)$ denotes the film thickness along the central axis. The liquid profile is well described by a parabolic curve when viewed in cross-section. (c) Optical micrograph of PDMS spreading on a 300 μm wide hydrophilic stripe. Only a small segment of the reservoir pad and metal heater are visible on the left side.

Fig. 1(b). An optical micrograph of a spreading rivulet is shown in Fig. 1(c)—a small portion of the square reservoir pad appears to the left.

The liquid used in this study was polydimethylsiloxane (PDMS, Fluka), a silicone oil with viscosity $\mu = 20$ mPa s, density $\rho = 950$ kg/m^3 and surface tension $\gamma = 20.3$ mN/m at 22 °C.[21] The thermal coefficient $d\gamma/dT$ is -0.06 mN/m·K.[22] Additional material constants are the specific heat capacity $c_p = 1550$ J/kg·K and the thermal conductivity $k = 0.14$ W/m·K. Shown in Fig. 2 are the surface tension and viscosity of PDMS as a function of temperature. While the thermal coefficient $d\gamma/dT$ is essentially constant over the temperature range shown, the viscosity shows a nonlinear depen-
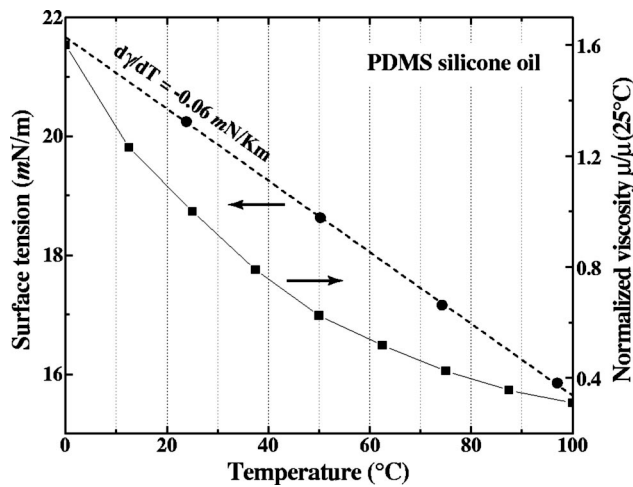
FIG. 2. Temperature dependence of the surface tension γ and normalized viscosity $\mu/\mu(25\,°C)$ for PDMS (Refs. 21, 22). $d\gamma/dT$ is essentially constant for the temperature range of the experiments (20 to 60 °C).

dence. The temperature range relevant to our experiments was 20° to 60 °C.

Linear temperature profiles were established along the microstripes by simultaneously powering an embedded resistive heater on one end of the sample and circulating cold water through a brass block to cool the opposite end. A typical measurement of the surface temperature profile along the length of a microstripe is shown in Fig. 3(a). The temperature variation is linear because the high thermal conductivity of the silicon substrate renders heat losses due to air convection or radiation insignificant. The inset [Fig. 3(b)] shows a comparison between experimental data (filled squares) and heat transfer simulations (solid line) for the dependence of
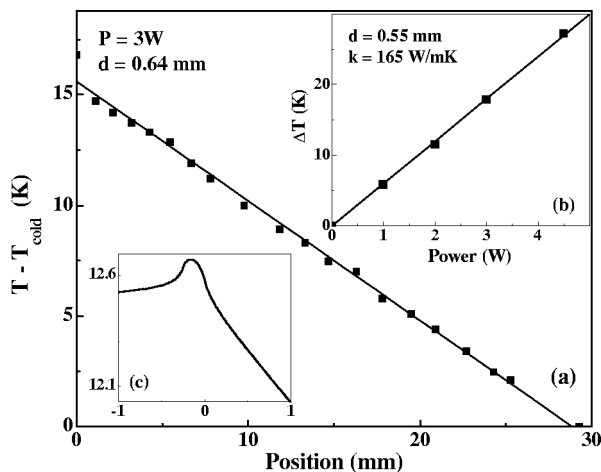

FIG. 3. (a) Measured temperature distribution along a hydrophilic stripe located near the center of the sample for a power input of 3W and a silicon wafer thickness of 640 μm. The solid line is a linear fit to the data. (b) Measured temperature difference $\Delta T = T_{hot} - T_{cold}$ as a function of input power for a silicon wafer thickness of 550 μm. The heating wire was located 28.4 mm from the edge of the brass block. The results of two-dimensional finite element simulations assuming a thermal conductivity $k_{Si} = 165$ W/m·K are represented by the solid line. (c) Results of finite element calculations of the temperature profile $T(x) - T_{cold}$ near the inlet $x=0$. The temperature is slightly higher directly above the 250 μm wide heating wire which produces a higher thermal gradient in the immediate vicinity of the inlet.

the maximum temperature difference $T_{hot} - T_{cold}$ (i.e., the temperature difference between opposite sides of the substrate), as a function of the heater input power. These finite element simulations were calculated from the thickness ($\hat{z}$) averaged steady-state heat conduction equation in the presence of a constant volumetric heat source (representing the activated heating resistor) and a constant reference temperature T_{cold} (representing the heat sink provided by the cooled brass block). Convective and radiative heat loss were incorporated through a convective heat transfer coefficient $h_{conv} = 7.5$ W/m^2 and a substrate thermal emissivity of 0.9, both of which provided only minor corrections to the thermal profile. The Si substrate thickness was $d_{Si} = 550$ μm.

Figure 3(c) shows results of the thermal distribution in the vicinity of the resistive heater at the stripe inlet. This distribution was computed from the width ($\hat{y}$) averaged heat conduction equation and the same boundary conditions as above. The local maximum in the surface temperature, which occurs directly above the resistive heater, gives rise to a slightly larger thermal gradient within a few hundred microns of the microstripe inlet.

Since the heating resistors did not span the entire (transverse) width of the sample [see the layout in Fig. 1(a)], the temperature gradient was slightly higher near the central portions of the sample than at the margins. The thermal gradients $|dT/dx|$ used in this study ranged from 0.1 to 1.1 K/mm and were determined by measuring the surface temperature at the reservoir inlet [see Fig. 1(a)] and above the brass block using an Omega iron–constantan thermocouple with a tip diameter of 130 μm. The error in the temperature measurements was estimated to be 0.4 °C.

The liquid sample was manually deposited onto the diamond shaped reservoirs using a Hamilton digital syringe with a resolution of 0.1 μl. The uncertainty in the metered volume V was about ± 0.15 μl. The liquid volume was deposited after the substrate had thermally equilibrated as monitored by the electrical resistance of the heating wire. The advancing position of the liquid front was tracked by light interferometry using an Olympus BX-60 microscope equipped with a wavelength bandpass filter centered at $\lambda = 535$ nm.

The experimental uncertainties in the determination of the front position and speed were estimated to be ± 20 μm and 1%. The relative position of the resistive heater relative to the stripe inlet for different samples was found to affect the front speed by several percent. The relative orientation of these two patterns is set during sample manufacture in the lithography step that defines the hydrophilic patterns. The manual alignment precision using masks printed with a high-resolution image setter was about 250 μm.

III. THEORETICAL DESCRIPTION

The surface tension of a liquid decreases in almost linear fashion with increasing temperature from the melting to the boiling point.[23] Variations in temperature along a direction $\hat{x}$ can therefore be used to generate a shear stress $\tau = d\gamma/dx = (d\gamma/dT) \cdot (dT/dx)$ at an air–liquid interface, which in-

duces flow from warmer to cooler regions.[24] In what follows, it is assumed that the temperature of the air–liquid interface is equal to the substrate temperature and that the thermal gradient is constant and parallel to the microstripe. Typical values for the Peclet and Biot numbers are $Pe = Uh\rho c_p/k_{liquid} \approx 0.05$ and $Bi = h_{conv}h/k_{liquid} \approx 0.003$ for a characteristic flow speed $U \approx 100 \ \mu m/s$, a heat coefficient $h_{conv} = 7.5 \ W/m^2 \cdot K$ for natural convection, and film height $h \approx 50 \ \mu m$. These values indicate that vertical temperature variations within the liquid film can be ignored.

A. Thermocapillary flow on homogeneous substrates

Levich[24] first established the hydrodynamic equations describing thermocapillary motion in thin liquid films. For sufficiently thin and flat films (i.e., vanishing Bond and capillary numbers) subject to a constant stress τ, the average flow speed is given by $U = h\tau/2\mu$. Ludviksson and Lightfoot[25] later examined the climbing of a liquid film along a vertical substrate whose heated end was immersed in a pool of completely wetting liquid. Interferometric measurements of the steady state film profiles showed good agreement with their theoretical model for all but the thinnest films.[26] More recently, Carles and Cazabat[27] and Fanton *et al.*[28] have focused on the role of the meniscus curvature (where the climbing film merges with the liquid bath) in determining the entry film thickness.

The scaling laws governing the entrained film thickness in the nonisothermal case can be obtained by analogy with the Landau–Levich dip-coating problem[29] for which $h \sim l \ Ca^{2/3}$, where $l = \sqrt{\gamma/\rho g}$ is the capillary length and $Ca = \mu U/\gamma$ is the capillary number. Substituting $U = h\tau/2\mu$ for the coating speed, Carles *et al.* and Fanton *et al.* showed that the asymptotic film thickness away from the meniscus scales as $h_\infty \sim l^3\tau^2/\gamma^2$. The flow velocity therefore scales as $U \sim l^3\tau^3/\mu\gamma^2$, which is a strong function of the applied shear stress. For higher thermal gradients and correspondingly thicker films where gravitational drainage is significant, the characteristic flow speed instead scales as $U \sim \tau^2/\rho g$.

It has been shown in a number of studies[15–17,25] that thin liquid films spreading on a non-isothermal substrate develop a capillary ridge near the contact line. This ridge undergoes a fingering instability like that observed in films flowing down an inclined plane[30,31] and centrifugally driven films.[32,33] For thermocapillary spreading, the wavelength associated with the most unstable mode is given by $\Lambda = 18h/(3 \ Ca)^{1/3}$ provided the surface is smooth, homogeneous and completely wetted by the liquid.

B. Thermocapillary flow on hydrophilic stripes

The study of driven flows on chemically heterogeneous substrates is relatively new. Recent interest has focused on systems in which there exist two competing wavelengths—one established by the hydrodynamic forces, the other established by the feature size of the substrate pattern. For example, by templating a silicon surface with hydrophobic microstripes consisting of a self-assembled monolayer of octadecyltrichlorosilane (OTS), one can impose an "external" wavelength on thermocapillary driven flow.[34] Studies on

such patterned substrates have revealed undulations at the moving front whose wavelength matches that of the underlying stripe pattern for stripe widths $w > 50 \ \mu m$. Below this width, the wavelength of the liquid front reverts back to the value consistent with the most unstable hydrodynamic mode obtained with chemically homogeneous surfaces. These experiments also showed that the thermocapillary flow was slower on the OTS treated stripes. The OTS coated regions did not prevent liquid migration altogether as required for the present study.

In all previous studies of thermocapillary spreading, the spatial dependence of the viscosity has been neglected since the extent of spreading was normally much less than a centimeter. In what follows, the distances traversed are several centimeters. The variation in viscosity with distance is therefore included in the numerical simulations. Polynomial fits to the data shown in Fig. 2 are given in Ref. 35.

In this section we derive the lubrication equations for the flow speed and film height of a Newtonian liquid on a hydrophilic microstripe subject to a constant longitudinal thermal gradient. Similar equations have been derived for the spreading of a rivulet down an inclined, chemically homogeneous substrate, including the presence of a contact line at the moving front.[36,37] We approximate the flow as unidirectional; deviations to this approximation caused by the junction between the diamond shaped reservoir and the narrow hydrophilic stripe are ignored. The equations are derived in the limit of small Ca and vanishing Bond number $Bo = \rho g w^2/\gamma$. Figure 1(b) depicts a close-up of the flow geometry. The x-axis coincides with the stripe center, the y-coordinate spans the width of the stripe $[-w/2,+w/2]$, and the z-axis lies normal to the substrate surface. The variable $h_c(x,t)$ denotes the film thickness along the stripe centerline axis. With these approximations, the Navier–Stokes equations reduce to

$$\frac{\partial p}{\partial x} = \mu \frac{\partial^2 u}{\partial z^2}, \tag{1}$$

$$\frac{\partial p}{\partial y} = \mu \frac{\partial^2 v}{\partial z^2}, \tag{2}$$

$$\frac{\partial p}{\partial z} = 0, \tag{3}$$

where u and v denote the streamwise and transverse velocity fields, respectively. The boundary conditions for these equations are

$$u(x,y,0) = 0, \tag{4}$$

$$v(x,y,0) = 0, \tag{5}$$

$$\mu \frac{\partial u}{\partial z}(z=h) = \tau, \tag{6}$$

$$\mu \frac{\partial v}{\partial z}(z=h) = 0, \tag{7}$$

$$p(x,y,z=h) = -\gamma\left(\frac{\partial^2 h}{\partial x^2} + \frac{\partial^2 h}{\partial y^2}\right). \tag{8}$$

These conditions reflect the no-slip condition at the liquid–solid interface and a constant streamwise shear stress τ at the air–liquid interface. The expression for the capillary pressure p assumes interfacial shapes with small slope. The streamwise and transverse velocity fields are then given by

$$u(x,y,z) = \frac{1}{\mu}\left[\frac{\partial p}{\partial x}\left(\frac{z^2}{2} - zh(x,y)\right) + \tau z\right], \tag{9}$$

$$v(x,y,z) = \frac{1}{\mu}\frac{\partial p}{\partial y}\left(\frac{z^2}{2} - zh(x,y)\right), \tag{10}$$

where μ depends on position because of the temperature variation along the liquid–solid interface. The kinematic condition, which requires dh/dt to equal the surface flow speed normal to the air–liquid interface, leads to the evolution equation for the film thickness,

$$\frac{\partial h}{\partial t} + \boldsymbol{\nabla} \cdot \mathbf{Q} = 0, \tag{11}$$

where $\mathbf{Q} = (Q_x, Q_y)$ is a vector representing the volumetric flow rate per unit width. Away from the liquid inlet and spreading front, the flow field is essentially unidirectional and $Q_y = 0$. Within the lubrication approximation, this implies that $\partial p/\partial y = 0$. For microstreams whose length far exceeds the width, $\partial/\partial y(\partial^2 h/\partial x^2) \ll \partial/\partial y(\partial^2 h/\partial y^2)$. This condition therefore defines an interfacial shape with constant transverse curvature, namely $h(x,y,t) = h_c(x,t)(1 - 4y^2/w^2)$. Numerical simulations not assuming this parabolic profile show hardly any deviations from results obtained with this simplified form.

Substituting the flow rate,

$$Q_x(x,y,t) = \int_0^h u(x,y,z,t)\,dz, \tag{12}$$

into Eq. (11) yields

$$\frac{\partial h}{\partial t} + \frac{\partial}{\partial x}\left[\frac{\tau h^2}{2\mu} + \frac{h^3}{3\mu}\frac{\partial}{\partial x}(\gamma\nabla^2 h)\right] = 0. \tag{13}$$

Integration of this expression with respect to y using $h(x,y,t) = h_c(x,t)(1 - 4y^2/w^2)$ yields the equation for the centerline height (the subscript c is omitted henceforth),

$$\frac{\partial h}{\partial t} + \frac{\partial}{\partial x}\left[\frac{2\tau h^2}{5\mu} + \frac{64 h^3}{315\mu}\frac{\partial}{\partial x}(\gamma h_{xx}) - \frac{64 h^3}{35 w^2\mu}\frac{\partial}{\partial x}(\gamma h)\right]$$
$$= 0. \tag{14}$$

The surface tension and viscosity are both position dependent due to the presence of the thermal gradient as shown in Fig. 2.

Equation (14) is nondimensionalized by introducing the following variables:

$$\bar{h} = \frac{h}{h_0},\ \xi = \frac{x}{l_c},\ \bar{t} = \frac{t U_c}{l_c},\ \bar{\gamma} = \frac{\gamma}{\gamma_0} \text{ and } \bar{\mu} = \frac{\mu}{\mu_0}, \tag{15}$$

where h_0, γ_0 and μ_0 denote the centerline height, the surface tension and the viscosity of the liquid film at the inlet position $x = 0$. The characteristic flow speed set by the thermocapillary forces is given by

$$U_c \equiv \frac{2 h_0 \tau}{5\mu_0}. \tag{16}$$

The characteristic length scale in the streamwise direction, chosen to reflect the balance between capillary and thermocapillary forces, is set by

$$l_c \equiv \sqrt[3]{\frac{h_0^3}{3\mathsf{Ca}}}, \tag{17}$$

where $\mathsf{Ca} = \mu_0 U_c/\gamma_0$. This dynamic lengthscale is the same as that previously used in studies of thermocapillary flow[26,38] and gravitationally driven flow on homogeneous surfaces.[39] The final equation governing liquid flow on the heated channel becomes

$$\frac{\partial\bar{h}}{\partial\bar{t}} + \frac{\partial}{\partial\xi}\left(\frac{\bar{h}^2}{\bar{\mu}}\right) + \frac{64}{105}\frac{\partial}{\partial\xi}\left[\frac{\bar{h}^3}{\bar{\mu}}\frac{\partial}{\partial\xi}\left(\bar{\gamma}\frac{\partial^2\bar{h}}{\partial\xi^2}\right)\right]$$
$$-\frac{192}{35}N_D\frac{\partial}{\partial\xi}\left[\frac{\bar{h}^3}{\bar{\mu}}\frac{\partial}{\partial\xi}(\bar{\gamma}\bar{h})\right] = 0, \tag{18}$$

where the parameter $N_D \equiv (l_c/w)^2$ represents the square of the ratio of the dynamic length scale l_c and the geometric length scale w.

The third term in Eq. (18) defines the contribution to the flow rate stemming from the variation in longitudinal surface curvature (i.e., along the $\hat{\xi}$-axis). The influence of this capillary term has been studied extensively in the context of the spreading of isothermal droplets.[40] The term proportional to N_D defines the capillary contribution from streamwise variation in the transverse surface curvature due to the liquid confinement by the chemical patterning. This term only involves the first derivative of the film height since the liquid cross-sectional shape is assumed to be a parabola. The influence of this term on the spreading of isothermal rivulets on hydrophilic microstripes has already been investigated.[41] Depending on the detailed shape of the liquid film entering the microstripe, this term can either increase or decrease the initial spreading speed.

Equation (18) requires the specification of four boundary conditions and an initial condition. These are chosen to be $\bar{h}(\xi=0,\bar{t})=1$, $\partial\bar{h}/\partial\xi(0,\bar{t})=0$, $\bar{h}(\xi_n,\bar{t})=b=1/200$ and $\partial\bar{h}/\partial\xi(\xi_n,\bar{t})=0$, where ξ_n is the rightmost boundary of the computational domain $[0,\xi_n]$. The limiting film thickness b, which represents a flat precursor film ahead of the contact line, eliminates the stress singularity in problems with a moving contact line.[40] A detailed discussion of contact line models and their effect on the film profile and dynamical contact and angles can be found in Refs. 38, 42, and 43.

The initial condition for the film shape at $\bar{t}=0$ is given by $\bar{h}(\xi,0)=[(1+b)-(1-b)\tanh(\xi-\xi_o)]/2$, where ξ_o denotes the inlet position. The boundary conditions at $\xi=0$ predicate a constant and flat inlet height. In practice, the capillary and hydrostatic pressure exerted by the liquid
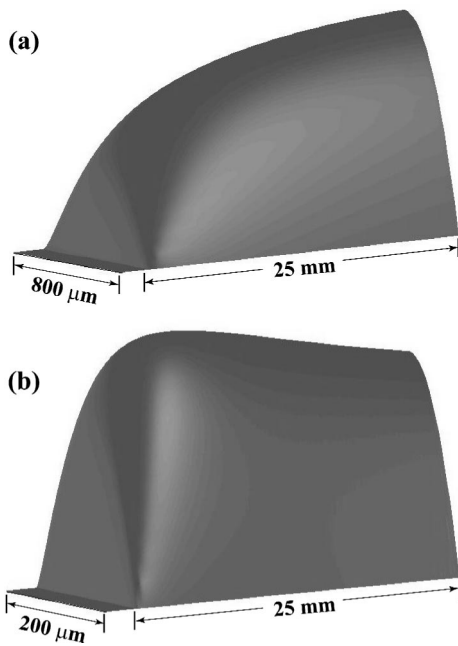
(a)

(b)

FIG. 4. Numerical solutions of Eq. (18) for thermocapillary spreading of PDMS on a completely wetting microstripe. (a) $w = 800$ μm, $dT/dx = 0.20$ K/mm and $h_0 = 56$ μm ($N_D = 6.0$). For large widths and smaller gradients, the height profile decreases monotonically toward the advancing front and no capillary ridge is visible. (b) $w = 200$ μm, $|dT/dx| = 1.4$ K/mm and $h_0 = 12$ μm ($N_D = 1.8$). For smaller widths and larger gradients, the film height increases monotonically toward the advancing front.

sample on the reservoir pad, as well as the local maximum of the surface temperature directly above the heating resistor [see Fig. 3(c)] can modify the initial film thickness and shape in ways not perfectly represented by the boundary conditions we used, especially for large thermal gradients.

Besides the boundary and initial conditions, solution of Eq. (18) requires the specification of N_D, $\bar{\mu}$ and $\bar{\gamma}$. The specification of N_D further requires the values of w, τ, μ_0, γ_0 and h_0. All the required parameters were obtained directly from experiment except for the inlet film height h_0. In our experiments, the inlet height was too large to measure with optical interferometry and was therefore treated as a (constant) fitting parameter. The entry film thickness h_0 may decrease in time for large thermal gradients and wide microstripes. In principle, this parameter cannot be specified independently but is determined by the reservoir geometry, the liquid volume and the ratio of thermocapillary to capillary forces. The simulations therefore capture the behavior of the liquid film once it has spread a distance $L \gg w$.

The influence of the parameter N_D on solutions of Eq. (18) is shown in Fig. 4 for 25 mm long rivulets. For the larger stripe width and smaller thermal gradient [Fig. 4(a)] where $N_D = 6.0$, the film thickness decreases monotonically from the inlet to the spreading front. This profile is similar to the shapes obtained for isothermal capillary spreading on hydrophilic microstripes.[41] For the smaller width and larger gradient [Fig. 4(b)] where $N_D = 1.8$, the thermocapillary force is more pronounced. In this case, the film height increases monotonically from the inlet to the front position in a ramp-like fashion.

For long rivulet extensions $\xi \gg 1$, the capillary contributions in Eq. (14) scale as $\epsilon^3 h$ and $\epsilon h(h/w)^2$ ($\epsilon \equiv h/L \ll 1$), whereas the thermocapillary term scales as h^2. In this limit, the flux is dominated by the thermocapillary term. In steady state, the flux is a constant, leading to the equality $\bar{h}^2/\bar{\mu} = 1$. Approximating the viscosity by the linear function $\bar{\mu}[T(\xi)] = (1 + a\xi)$ dictates a centerline profile of the form $\bar{h}(\xi) = \sqrt{1 + a\xi}$. Consequently the average flow speed is given by

$$\bar{u}(\xi) = \frac{5}{4} \frac{1}{\sqrt{1 + a\xi}}, \tag{19}$$

where $\bar{u}(\xi) = u(x)/U_c$. The increase in viscosity near the cooler edge causes a slowdown in speed but an increase in film height such that the overall flow rate remains constant.

C. Scaling relations

Determination of the actual value of the inlet height h_0 as a function of w, τ and V requires a full asymptotic matching of the reservoir region to the channel dynamics. There are two limiting cases, however, in which scaling relations can be easily derived, namely when h_0 is controlled by the capillary and/or hydrostatic pressure on the reservoir or by the thermocapillary stress along the microstripe.

For small thermal gradients and large reservoir volumes, the inlet height h_0 is dominated by the reservoir pressure. The inlet height for isothermal spreading[41] scales as $h_0 \sim w^2 V$. Substituting this relation into Eq. (16) gives $U_c \sim w^2 V \tau / \mu_0$. In this limit, the flow speed scales quadratically with the stripe width and linearly with the reservoir volume and applied thermal gradient.

For large thermal gradients and small reservoir volumes, the inlet height is governed by the thermocapillary stress along the microstripe. In a separate study of Newtonian liquids entrained at constant speed on hydrophilic microstripes,[44] it was shown that the presence of significant transverse curvature strongly modifies Landau's[29] original relation between the film thickness and capillary number (described in Sec. III A). In particular, $h_0 \sim w \, Ca^{1/3}$. Substituting this dependence into Eq. (16) predicts that $U_c \sim w^{3/2} \tau^{3/2}/(\mu_0 \gamma_0^{1/2})$. In either case, the dependence of the flow speed on the applied stress τ is significantly weaker than that derived for vertically climbing films on homogeneous substrates.[27]

IV. EXPERIMENTAL RESULTS AND DISCUSSION

Figure 5 shows results of the rivulet front speed as a function of downstream position x for four different settings of the thermal gradient. The data were obtained with microstripe widths ranging from 200 to 700 μm. As expected, the flow is faster for larger values of $|dT/dx|$ and wider stripes. The speed was obtained by tracking the position of the first dark interference fringe. This fringe does not exactly correspond to the position of the contact line but is the closest marker to the front that can be measured reliably. In these experiments, the heating electrode and the cooling brass
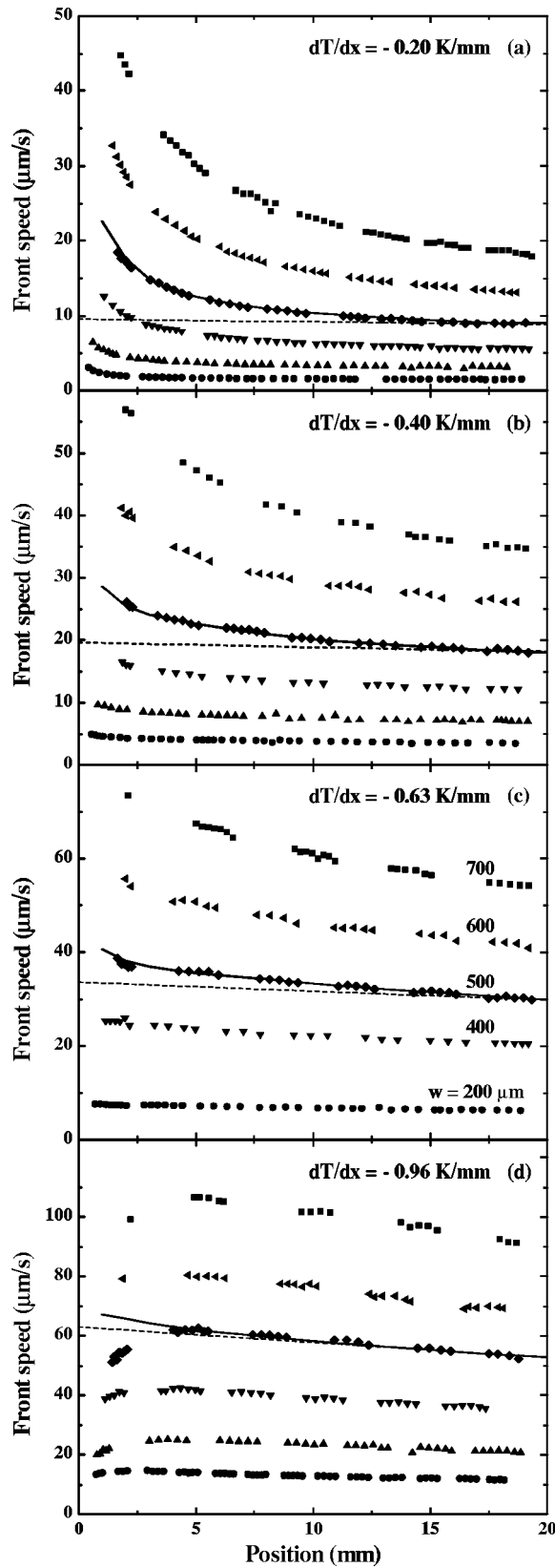
Phys. Fluids, Vol. 15, No. 5, May 2003

Thermocapillary actuation of liquid flow   1301

FIG. 5. Position dependence of the liquid front speed for stripe widths 200 (●), 300 (▲), 400 (▼), 500 (◆), 600 (◀) and 700 μm (■). The temperature gradients were (a) -0.20, (b) -0.40, (c) -0.63 and (d) -0.96 K/mm and the volume on the terminal reservoir was 8 μl. The solid lines are derived from numerical results of Eq. (18) for $w = 500$ μm. The fitted values of the inlet height h_0 were (a) 42.0, (b) 38.1, (c) 38.7 and (d) 41.8 μm. The dashed lines correspond to the constant flux solution given by Eq. (19).
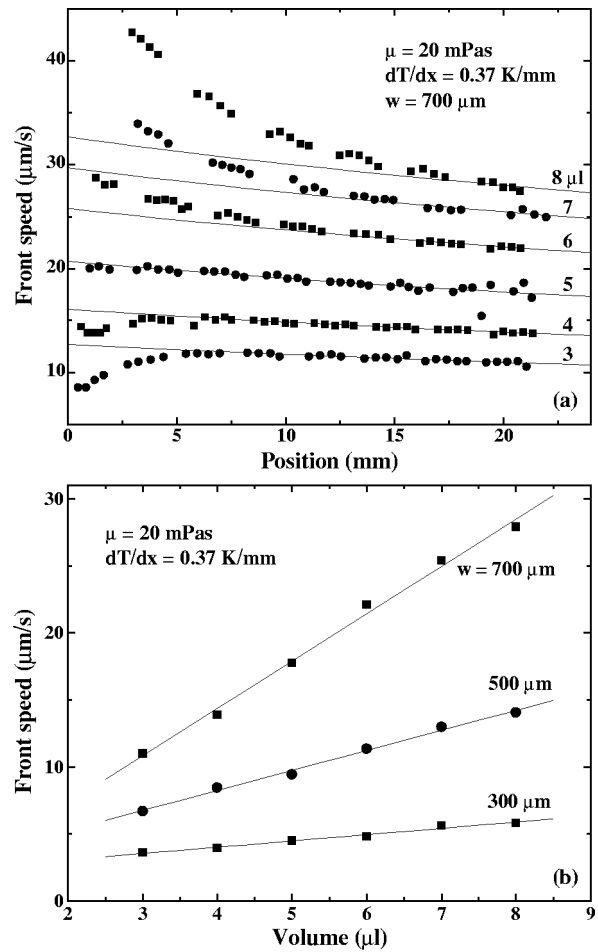

FIG. 6. (a) Position dependence of the liquid front speed for $w = 700$ μm, $|dT/dx| = 0.37$ K/mm and V ranging from 3 to 8 μl. The solid lines correspond to the constant flux solution given by Eq. (19). (b) Volume dependence of the front speed for stripe widths $w = 300$, 500 and 700 μm at $x = 20$ mm. The solid lines represent linear fits to the experimental data.

block were separated by a fixed distance of 28.4 mm. The shear stress induced in the liquid film ranged from 0.012 -0.058 Pa. The dashed lines shown in the figure represent constant flow rate solutions according to Eq. (19). The solid lines represent the flow speed extracted from the full numerical solution to Eq. (18). The agreement between the measured data and the numerical solutions is generally excellent.

Except for the largest gradient used, the measured speed decreases monotonically with increasing distance. This decrease is due to three factors, namely the increase in liquid viscosity with decreasing temperature, the capillary contributions to the flow that diminish with increasing distance according to Eq. (14) and the slight depletion in reservoir volume with time. The flow speed in Fig. 5(d) shows an initial increase in speed which persists several millimeters from the inlet. This increase is suggested by the heat transfer simulations shown in Fig. 3(c) where the finite heater width and substrate thickness cause a local maximum in the surface temperature. Close to the inlet, the thermal gradient caused by this local maximum opposes the flow into the channel over a very short distance.

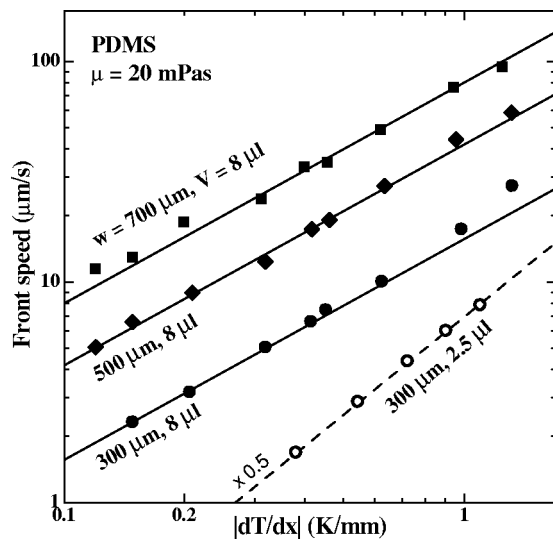The dependence of the flow speed u on the liquid reser-

FIG. 7. Liquid front speed as a function of $|dT/dx|$ for $V = 8$ μl and w = 300, 500 and 700 μm (filled symbols) measured at $x = 20$ mm. The solid lines correspond to a linear relation $u \sim |dT/dx|$. The open circles represents data obtained for $w = 300$ μm and $V = 2.5$ μl. The dashed line corresponds to the relation $u \sim |dT/dx|^{1.47}$. The measured values for $V = 2.5$ μl were divided by a factor of 2. All data have been corrected to compensate for the different viscosities $\mu[T(x=20 \text{ mm})]$ for different applied thermal gradients.

voir volume was also investigated. Figure 6(a) shows the front speed u as a function of x for $w = 700$ μm using sample volumes ranging from 3 to 8 μl. Smaller volumes and narrower stripes produce slower spreading. As the volume is reduced from 8 to 3 μl, the speed no longer decreases monotonically but exhibits the same initial acceleration as observed in Fig. 5(d). Figure 6(b) shows the volume dependence of the front speed for a 20 mm long rivulet on stripe widths $w = 300$, 500 and 700 μm. The dependence of speed on sample volume is essentially linear, consistent with the prediction in Sec. III C.

Figure 7 illustrates the dependence of flow speed at the fixed location $x = 20$ mm on the magnitude of the thermal gradient. The data are fitted by a relation of the form $u \sim |dT/dx|^{\beta}$ where $\beta = 1.0$ for the larger sample volume (8.0 μl) and $\beta = 1.47$ for the smaller volume (2.5 μl). The data for 8.0 μl and $w = 300$ μm show a transition to larger exponents at $|dT/dx| \gtrsim 1$ K/mm. The reduction in liquid volume changes the exponent from 1 to 3/2. In a previous study of isothermal spreading on hydrophilic microstripes, it was shown that the front speed strongly depends on the sample volume.[41] In particular, the speed of a PDMS sample deposited on a 4.5 mm square reservoir was found to scale as $V^{2.82}$. Consequently, reducing the volume from 8 to 2.5 μl diminishes the pressure exerted at the inlet by a factor of about 25. This decrease in inlet pressure biases the system toward the thermocapillary limit, as described in Sec. III C, for which $u \sim |dT/dx|^{3/2}$. The two limiting exponents observed in the experimental data are in good agreement with these scaling predictions and capture the transition between an inlet height dominated by the reservoir pressure and shear dominated flow.

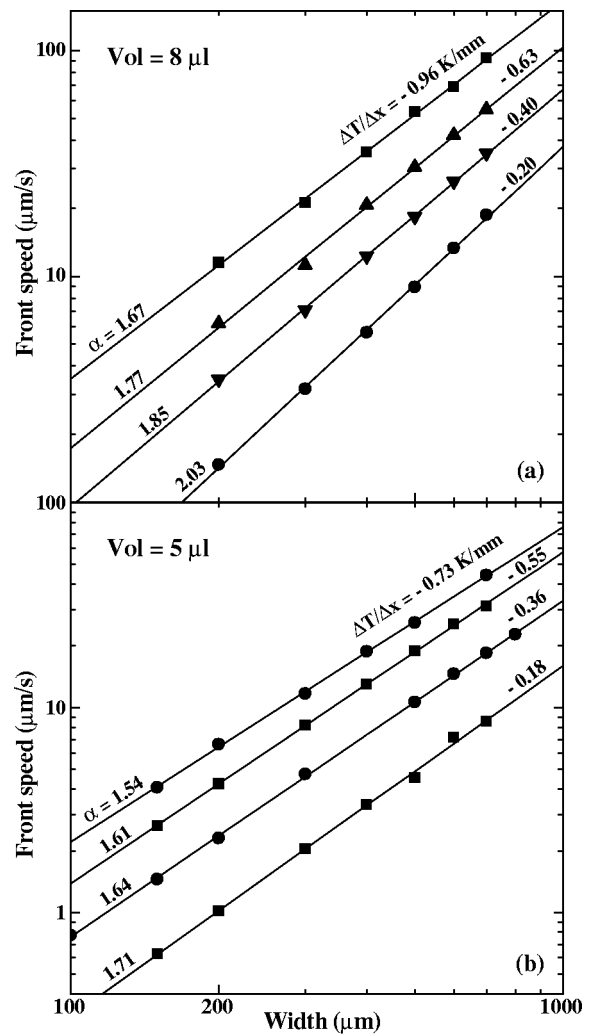The dependence of flow speed on w for two different

FIG. 8. Liquid front speed as a function of the stripe width for (a) $V = 8$ μl and (b) $V = 5$ μl at $x = 18$ mm. The data are well represented by power law relations $u \sim w^{\alpha}$ (solid lines). The exponent α ranges from 2 for small gradients and larger volumes to 3/2 for large gradients and smaller volumes.

sample volumes is shown in Fig. 8. The data shown in Fig. 8(a) were extracted from Fig. 5 at a location $x = 18$ mm. The rivulet is then sufficiently long for the thermocapillary stress to dominate the flow. The flow speeds can be fitted by the functional form $u \sim w^{\alpha}$, where α is found to vary with the magnitude of the applied thermal gradient. The exponent decreases systematically from a value of 2 at low gradients and high volumes to about 1.5 for high gradients and smaller reservoir volumes. These limiting values are again in good agreement with the scaling predictions in the preceding section.

The fastest spreading speed we have measured to date is 600 μm/s using a lower viscosity PDMS oil (5 cSt) on an 800 μm wide stripe with an applied gradient of $|dT/dx|$ = 1.44 K/mm and a liquid volume of 8 μl. Faster speeds can be obtained with liquids of smaller viscosity and larger $d\gamma/dT$. Narrower and continuously fed reservoirs will also increase the inlet film height such that speeds in excess of 1 mm/s appear accessible.

V. SUMMARY

We have studied thermocapillary flow generated by a constant thermal gradient along hydrophilic microstripes ranging in width from 100 to 800 μm. The microstripes are lithographically defined on a silanized silicon surface. The flow speed was measured as a function of the stripe width w, the applied thermal gradient $|dT/dx|$ and the volume V of liquid deposited on a terminal reservoir. Numerical solutions of the governing lubrication equations, including capillary effects due to the lateral confinement of the flowing liquid and the streamwise increase in viscosity, show excellent agreement with experimental results. In the limiting cases where the inlet film thickness is either dominated by the capillary and/or hydrostatic pressure at the terminal reservoir (small $|dT/dx|$ and large V) or by the thermocapillary stress along the microstripe (large $|dT/dx|$ and small V), the front speed scales as $w^{\alpha}|dT/dx|^{\beta}$. When the inlet height is dynamically controlled by the thermal stress, α and β both approach 3/2; when the inlet height is controlled by the reservoir pressure, $\alpha \to 2$ and $\beta \to 1$. The experimental data fall within these predicted values. Moreover, for long rivulet extensions, the capillary forces due to streamwise curvature become negligible and the liquid flux asymptotes to a constant value.

In this study we demonstrate that thermocapillary stresses provide a suitable means for routing liquid microstreams along lithographically defined pathways. An extension of this prototype assembly to a platform with electronically addressable microheater arrays, which allows for active control of flow speed, direction and timing, is currently being developed. With flow speeds of order 1 mm/s within reach, thermocapillary flow on patterned substrates holds promise for emerging applications in microfluidic delivery and transport.

ACKNOWLEDGMENTS

[1] D. Figeys, "Array and lab on a chip technology for protein characterization," Curr. Opin. Mol. Ther. **1**, 685 (1999).

[2] L. Bousse, C. Cohen, T. Nikiforov, A. Chow, A. R. Kopf-Sill, R. Dubrow, and J. W. Parce, "Electrokinetically controlled microfluidic analysis systems," Annu. Rev. Biophys. Biomed. Struct. **29**, 155 (2000).

[3] D. Meldrum, "Automation for genomics," Genome Res. **10**, 1288 (2000).

[4] G. J. M. Bruin, "Recent developments in electrokinetically driven analysis on microfabricated devices," Electrophoresis **21**, 3931 (2000).

[5] J. Pfahler, J. Harley, H. Bau, and J. Zemel, "Liquid transport in micron and submicron channels," Sens. Actuators A **21–23**, 431 (1990).

[6] A. Manz, C. S. Effenhauser, N. Burggraf, D. J. Harrison, K. Seiler, and K. Fluri, "Electroosmotic pumping and electrophoretic separations for miniaturized chemical analysis systems," J. Micromech. Microeng. **4**, 257 (1994).

[7] S. F. Bart, L. S. Tavrow, M. Mehregany, and J. H. Lang, "Microfabricated electrohydrodynamic pumps," Sens. Actuators A **21–23**, 193 (1990).

[8] W. Ritchie, "Experimental researches in voltaic electricity and electromagnetism," Philos. Trans. R. Soc. London **122**, 279 (1832).

[9] J. Jang and S. S. Lee, "Theoretical and experimental study of magnetohydrodynamic micropump," Sens. Actuators A **80**, 84 (2000).

[10] D. C. Duffy, H. L. Gillis, J. Lin, N. F. Sheppard, and G. J. Kellogg, "Microfabricated centrifugal microfluidic systems," Anal. Chem. **71**, 4669 (1999).

[11] T. S. Sammarco and M. A. Burns, "Thermocapillary pumping of discrete droplets in microfabricated analysis devices," AIChE J. **45**, 350 (1999).

[12] M. G. Pollack, R. B. Fair, and A. D. Shenderov, "Electrowetting-based actuation of liquid droplets for microfluidic applications," Appl. Phys. Lett. **77**, 1725 (2000).

[13] J. Lee and C.-J. Kim, "Surface-tension-driven microactuation based on continuous electrowetting," J. Microelectromech. Syst. **9**, 171 (2000).

[14] T. B. Jones, M. Gunji, M. Washizu, and M. J. Feldman, "Dielectrophoretic liquid actuation and nanodroplet formation," J. Appl. Phys. **89**, 1441 (2001).

[15] A. M. Cazabat, F. Heslot, S. M. Troian, and P. Carles, "Fingering instability of thin spreading films driven by temperature gradients," Nature (London) **346**, 824 (1990).

[16] A. M. Cazabat, F. Heslot, P. Carles, and S. M. Troian, "Hydrodynamic fingering instability of driven wetting films," Adv. Colloid Interface Sci. **39**, 61 (1992).

[17] J. B. Brzoska, F. Brochard-Wyart, and F. Rondelez, "Exponential growth of fingering instabilities of spreading films under horizontal thermal gradients," Europhys. Lett. **19**, 97 (1992).

[18] C. J. Glassbrenner and G. A. Slack, "Thermal conductivity of silicon and germanium from 3 K to the melting point," Phys. Rev. **134**, A1058 (1964).

[19] U. Srinivasan, M. R. Houston, R. T. Howe, and R. Maboudian, "Alkyltrichlorosilane-based self-assembled monolayer films for stiction reduction in silicon micromachines," J. Microelectromech. Syst. **7**, 252 (1998).

[20] B. C. Bunker, R. W. Carpick, R. A. Assink, M. L. Thomas, M. G. Hankins, J. A. Voigt, D. Sipola, M. P. de Boer, and G. L. Gulley, "The impact of solution agglomeration on the deposition of self-assembled monolayers," Langmuir **16**, 7742 (2000).

[21] *Datasheet for Wacker Silicone Fluids* (Wacker-Chemie GmbH, München, 2000).

[22] B. B. Sauer and G. T. Dee, "Molecular weight and temperature dependence of polymer surface tension. Comparison of experiment with theory," Macromolecules **24**, 2124 (1991).

[23] A. W. Adamson, *Physical Chemistry of Surfaces* (Wiley, New York, 1990).

[24] V. G. Levich, *Physicochemical Hydrodynamics* (Prentice–Hall, Englewood Cliffs, NJ, 1962).

[25] V. Ludviksson and E. N. Lightfoot, "The dynamics of thin liquid films in the presence of surface-tension gradients," AIChE J. **17**, 1166 (1971).

[26] D. E. Kataoka and S. M. Troian, "Stabilizing the advancing front of thermally driven climbing films," J. Colloid Interface Sci. **203**, 335 (1998).

[27] P. Carles and A. M. Cazabat, "The thickness of surface-tension-gradient-driven spreading films," J. Colloid Interface Sci. **157**, 196 (1993).

[28] X. Fanton, A. M. Cazabat, and D. Quere, "Thickness and shape of films driven by a Marangoni flow," Langmuir **12**, 5875 (1996).

[29] L. Landau and B. Levich, "Dragging of a liquid by a moving plate," Acta Physicochim. URSS **17**, 42 (1942).

[30] H. E. Huppert, "Flow and instability of a viscous current down a slope," Nature (London) **300**, 427 (1982).

[31] J. M. Jerrett and J. R. de Bruyn, "Fingering instability of a gravitationally driven contact line," Phys. Fluids A **4**, 234 (1992).

[32] F. Melo, J. Joanny, and S. Fauve, "Fingering instability of spinning drops," Phys. Rev. Lett. **63**, 1958 (1989).

[33] N. Fraysse and G. M. Homsy, "An experimental study of rivulet instabilities in centrifugal spin coating of viscous Newtonian and non-Newtonian fluids," Phys. Fluids **6**, 1941 (1994).

[34] D. E. Kataoka and S. M. Troian, "Patterning liquid flow on the microscopic scale," Nature (London) **402**, 794 (1999).

[35] Polynomial fits to the viscosity and surface tension data shown in Fig. 2 were extracted to be $\mu(T)$ [mPa s]$= 27.6755 - 0.3159T - 0.0032T^2 + 8.882 \times 10^{-5}T^3 - 4.806 \times 10^{-7}T^4$ and $\gamma(T)$ [mN/m]$= 21.5 - 0.06T$, where T is in degrees Celsius.

[36] L. W. Schwartz, "Viscous flows down an inclined plane—Instability and finger formation," Phys. Fluids A **1**, 443 (1989).

[37] D. T. Moyle, M. S. Chen, and G. M. Homsy, "Nonlinear rivulet dynamics during unstable wetting flows," Int. J. Multiphase Flow **25**, 1243 (1999).

[38] D. E. Kataoka and S. M. Troian, "A theoretical study of instabilities at the advancing front of thermally driven coating films," J. Colloid Interface Sci. **192**, 350 (1997).

[39] S. M. Troian, E. Herbolzheimer, S. A. Safran, and J. F. Joanny, "Fingering instabilities of driven spreading films," Europhys. Lett. **10**, 25 (1989).

[40] P. G. de Gennes, "Wetting: Statics and dynamics," Rev. Mod. Phys. **57**, 827 (1985).

[41] A. A. Darhuber, S. M. Troian, and W. W. Reisner, "Dynamics of capillary spreading along hydrophilic microstripes," Phys. Rev. E **64**, 031603 (2001).

[42] J. M. Davis, B. J. Fischer, and S. M. Troian, "A general approach to the linear stability of thin spreading films," in *Interfacial Fluid Dynamics in Physiochemical Phenomena*, Lecture Notes in Physics (Springer-Verlag, Berlin, 2003).

[43] J. M. Davis and S. M. Troian, "Influence of attractive van der Waals interactions on the optimal excitations in thermocapillary-driven spreading," Phys. Rev. E **67**, 016308 (2003).

[44] A. A. Darhuber, S. M. Troian, J. M. Davis, S. M. Miller, and S. Wagner, "Selective dip-coating of chemically micropatterned surfaces," J. Appl. Phys. **88**, 5119 (2000).